Research Square

Preprints are preliminary reports that have not undergone peer review.
They should not be considered conclusive, used to inform clinical practice,
or referenced by the media as validated information.

Experimental Analysis of Multiple Emulsion Compound Droplet Dynamics in a Stenosed Microchannel

Kumar Amit
Indian Institute of Technology Patna
Ashwani Assam
Indian Institute of Technology Patna
Abhishek Raj
araj@iitp.ac.in

Indian Institute of Technology Patna

correspondence

Keywords:

Posted Date: March 10th, 2026

DOI: https://doi.org/10.21203/rs.3.rs-8608391/v1

License: This work is licensed under a Creative Commons Attribution 4.0 International License.
Read Full License

Additional Declarations: No competing interests reported.

Experimental Analysis of Multiple Emulsion Compound Droplet Dynamics in a Stenosed Microchannel

Kumar Amit, Ashwani Assam, and Abhishek Raj*

Department of Mechanical Engineering, IIT Patna, Patna-801106, India

*Corresponding author; araj@iitp.ac.in

Abstract

The dynamics of (O/W)/O multiple emulsion droplets navigating through stenosed microchannels are critical for understanding droplet behaviour in confined geometries, with implications for drug delivery, controlled emulsification, and biomedical modelling. This study explores how factors such as flow rate ratio (Q_r), droplet size (both inner and outer), channel wall compliance, and the inherent size variation of the inner droplets influence the transit phenomena. Experimental results reveal that the size and transit time of the compound droplets varies exponentially with an increase in flow rate ratio ($3 \leq Q_r \leq 5$). Material optimization showed that Xanthan gum (XG) concentration ($0.16 - 0.2\%$ w/v) and intermediate oil concentrations ($\sim 15\%$ v/v) were found to stabilize the inner emulsions while maintaining consistent droplet behaviour. For larger inner droplets ($0.65 \leq D^*_{i,max} \leq 1.11$), mean transit times (for droplet passage through stenosed microchannel) were 52.27 ± 1.07 ms, approximately 8% higher than for smaller droplets ($0.21 \leq D^*_{i,max} \leq 0.25$) at 48.35 ± 0.96 ms. Crucially, wall compliance significantly altered droplet behaviour, leading to earlier droplet formation and consistently longer transit times due to curvature effects arising from wall deformation. The compliant channel exhibits a maximum t_{total} increase of 35.07% compared to the rigid channel at $Q_r = 3.333$. Additionally, this work practical preparation method for mineral oil emulsions using an XG+DI solution, which enables stable, foam-free visualization and controlled encapsulation. This novel preparation technique, combined with experimental insights, highlights the importance of both internal droplet structure and wall compliance in microfluidic droplet dynamics.

1 Introduction

The study of compound droplet dynamics in microfluidic systems has gained significant attention due to its relevance in applications such as drug delivery[1,2], controlled emulsification[3,4], and modelling of flow behaviour in confined geometries[2,5–8]. Microchannels with stenosed regions provide an ideal platform to investigate the behaviour of compound droplets under varying flow conditions, material properties, and geometric constraints. Compound droplets, which consist of an outer shell encapsulating one or more inner cores, exhibit complex deformation and transit dynamics that are influenced by multiple factors, including viscosity ratios, interfacial tension, and channel geometry. Understanding these dynamics is crucial for optimizing microfluidic systems for practical applications, such as targeted drug delivery and in vitro modelling of vascular diseases. However, the specific fluid-mechanical parameters that precisely govern the controlled encapsulation of multi-layered droplets for chemical applications, such as bespoke micro-reactors, remain to be fully characterized.

In recent years, several studies have focused on the behaviour of compound droplets in confined microchannels. Ho et al.[9] investigated the dynamics of compound droplets navigating obstacles in microchannels using front-tracking simulations validated against experimental data. Their findings highlighted the role of Weber number, capillary number, and obstacle geometry in determining droplet breakup modes. Similarly, Vu et al.[6] explored the deformation patterns of compound droplets in wavy constricted channels and demonstrated how Reynolds number, capillary number, and droplet size influence non-breakup versus breakup transitions.

The influence of material properties on compound droplet behaviour has also been extensively studied. Sattari et al.[5] analyzed migrating compound droplets in shear-thinning fluids within microcapillary tubes, demonstrating how rheological properties affect deformation patterns and shear stress behavior. Wang et al.[10] investigated double emulsion droplets under shear flow, identifying critical shear rates for stable deformation without breakup. Ren et al.[11] studied nanofluid-encapsulated double emulsion droplets under thermal conditions, showing that increasing temperature reduces interfacial tension and enhances deformation.

Channel geometry plays a pivotal role in governing compound droplet dynamics. Ho et al.[12] simulated multi-core compound droplets in ratchet microchannels and demonstrated how shell droplet size and neck region size impact transit time. Nguyen et al.[13] analysed indentation

formation on trailing surfaces of compound droplets flowing through constricted tubes, emphasizing the effects of capillary number and constriction depth on deformation patterns.

Leong et al.[14] numerically investigated the entry phenomena of a compound droplet through a two-dimensional rigid confinement, emphasizing the importance of material properties such as viscosity and surface tension on the droplet's entry behaviour. Their model focused on Newtonian droplet behavior and provided valuable insights into the mechanics of entry, while simplifying the system by not explicitly modeling the lubrication film between the droplet and the channel wall. Hashem et al.[7] employed adaptive-mesh-refinement techniques to model circulating tumour cells as compound droplets, highlighting the effects of the nucleus-to-cytoplasmic ratio on flow behaviour. Che et al.[15] simulated axisymmetric microchannels to study flow patterns and multi-layered droplet dynamics under varying capillary numbers. Gounley et al.[16] conducted fluid-structure interaction simulations to analyse the deformation patterns of simple and compound capsules under various flow conditions.

The passage of such droplets through tight constrictions is fundamentally governed by the formation of a thin lubrication film between the droplet and the channel wall, a phenomenon first described by Bretherton[17]. The pressure drops required to propel the droplet is highly sensitive to this film's thickness, which is a function of the capillary number (Ca). Our study explores how this classical framework is modulated by two key complexities: (1) the non-Newtonian, multi-layered internal rheology of a multiple emulsion, and (2) the mechanical compliance of the channel wall itself. In practical multiple-emulsion systems, the inner dispersed phase is often inherently polydisperse, particularly when generated via bulk emulsification. Rather than treating this variability as experimental noise, previous studies have demonstrated that dominant internal length scales can serve as meaningful first-order descriptors of compound droplet deformability and transport behaviour in the absence of detailed compound-droplet rheology. [7,14,18]

Building upon these findings and our previous investigation of single-phase droplet migration in stenosed microchannels, this study focuses on encapsulated compound droplets under varying flow conditions and material properties, an area that, to the best of the authors' knowledge, remains largely unexplored. By analysing the transit time (i.e., the time taken by droplets to pass through the stenosed region), deformation, and interaction of these droplets with compliant and rigid channel walls, we aim to refine our understanding of the mechanics governing biological cell migration in constricted vessels. Furthermore, we utilize the inherent

size variation of the inner droplets as a variable to examine how internal confinement scales impact the overall dynamics. The novelties of this study are as follows:

i. While XG is a known stabilizer, its application for preparing mineral oil emulsions with high optical clarity for micro-visualization studies, which are often hindered by foam or opacity from traditional surfactants, represents a key practical advancement investigated in this work
ii. Transitions from single-phase to encapsulated compound droplets, providing a more realistic multi-layered model.
iii. Systematic study of xanthan gum (0.16–0.2% w/v) and oil concentration (~15% v/v) for improved emulsion stability.
iv. Comparative analysis of compound droplet migration through rigid vs. compliant channels, emphasizing curvature-induced resistance on transit dynamics.
v. Investigation of factors affecting inner droplet encapsulation and its impact on total transit time.
vi. An experimental investigation testing the effect of various parameters (flow rate ratio, droplet size, wall compliance) to provide a robust understanding of compound droplet dynamics in deformable stenosed microchannels.

The experimental approach, which not only builds on previous findings but also provides fresh insights into the behaviour of compound droplets in stenosed channels, a topic that holds promise for enhancing the performance and reliability of microfluidic systems in a range of applications. By integrating modifications in emulsion preparation with a detailed analysis of transit time under varying flow conditions, this research aims to provide a closer approximation to biological cell dynamics in stenosed arteries. The findings could significantly impact biomedical applications, particularly in the development of more precise in vitro models for studying cardiovascular diseases and optimizing drug delivery strategies. In addition to biomedical analogues, compound droplets in microchannels also function as isolated microreactors, where droplet transit time and deformation directly influence residence time, mixing, and reaction yield in droplet-based chemical processes[19–21].

The work is structured as follows: Section 2 details materials and methods, including emulsion preparation, experimental setup. Sections 3.1 analyse flow rate ratios and size of inner droplets on transit time. Section 3.2 explores the factors influencing the number of encapsulated droplets, Section 3.3 examines the effect of wall compliance on transit and compares it with the transit time in rigid channels. Finally, Section 4 concludes the work by summarizing key findings. This

study provides a comprehensive framework for tailoring compound droplet behaviour in constrained environments, extending the utility of microfluidic systems in biomedical and industrial contexts while addressing limitations identified in earlier investigations.

2 Materials and Methods

2.1 Preparation of Base Solution and Emulsions

The base solution for this study was prepared using xanthan gum (XG) and deionized (DI) water. In five steps, the emulsion preparation was done, as shown in Fig. 1. Xanthan gum, a natural polysaccharide, was selected due to its ability to enhance the stability of emulsions[22,23]. The preparation process involved adding the desired proportion of XG to 45 mL of DI water, followed by vigorous shaking to ensure uniform mixing. The solution was then left undisturbed for 24 hours to allow complete hydration of the XG molecules, ensuring optimal viscosity and homogeneity.

After 24 hours, 7.5 mL of the hydrated XG + DI solution was taken in a 15 ml test tube, and the desired quantity of either mineral oil or mustard oil was added to it. The mixture was subjected to gentle manual shaking for 20–25 cycles, which proved sufficient to produce a stable emulsion. Air bubbles trapped during this process were carefully removed by gently rotating the tube on a horizontal axis, which allowed them to migrate to the walls and burst. Notably, no small-molecule surfactants (like Tween 80 or Span 80) were used in this preparation. Xanthan gum itself acted as the primary polymeric stabilizer, which alone provided adequate stabilization.

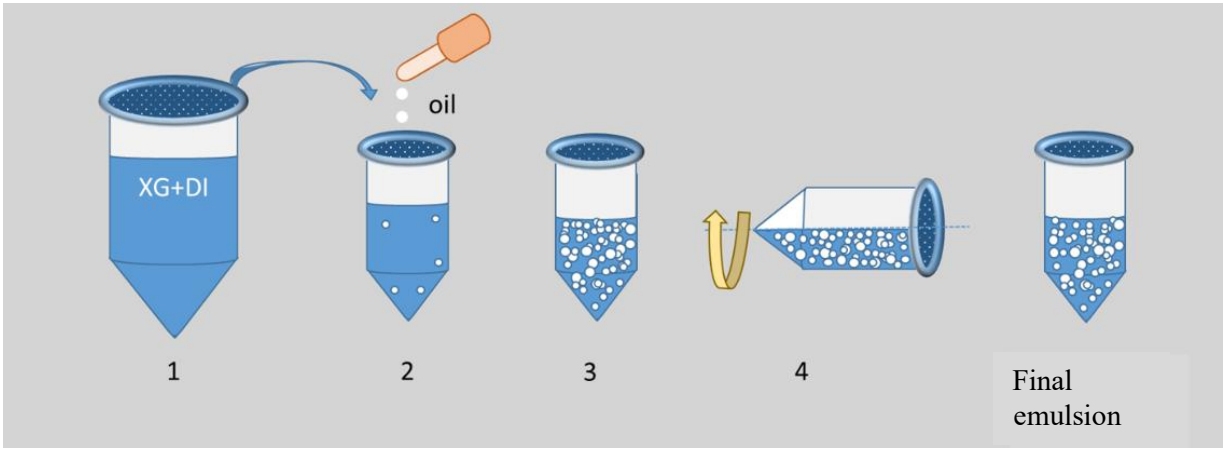


Fig. 1: Steps for emulsion preparation: a unique way with mineral oil.

This XG-based method was chosen specifically for its practical advantages in micro-visualization over traditional surfactants. As detailed in Appendix A, emulsifiers like Tween 80 or Span 80 generate significant, persistent foam that interferes with optical visibility. In contrast,

our XG+DI solution produced negligible foam and maintained excellent optical clarity, ensuring unobstructed visibility during the flow experiments.

Therefore, the XG+DI solution provided a simple yet effective method for preparing stable, foam-free emulsions suitable for microfluidic analysis. Its superior practical performance in terms of optical clarity and minimal foam, when compared to traditional surfactant-based methods (as detailed in Appendix A), made it the ideal choice for this study. While XG is a known stabilizer for other materials, such as such as with starch[24] and soybean oil[23], its use for creating mineral oil-based (O/W)/O multiple emulsions for flow visualization in stenosed microchannels represents a key practical novelty of this work.

2.1.1 Role of Xanthan Gum Concentration in Emulsion Preparation

Xanthan Gum (XG) is a widely used polysaccharide known for its ability to modify the rheological properties of aqueous solutions[14]. The concentration of XG in the continuous phase significantly impacts emulsion stability through its effect on solution viscosity and droplet interactions[22,25,26]. In this study, XG concentration in DI water was systematically varied to investigate its impact on emulsion formation and stability.

The results demonstrate that XG concentration plays a critical role in determining the solution's ability to stabilize oil droplets and maintain a uniform dispersion. Significant variations in emulsion properties were observed across the tested concentration range of 0.08% to 0.267% (w/v), as summarized in **Table 1**.

Our experimental observations reveal distinct behavior at different concentration regimes. At low XG concentrations (0.08% w/v), the solution exhibits negligible stability, with oil droplets immediately rising to the surface (see Fig. 2), indicating insufficient viscosity to overcome buoyancy forces. This aligns with previous findings that a critical concentration of xanthan gum (approximately 0.12-0.15% w/v) is necessary for effective emulsion stabilization[27].

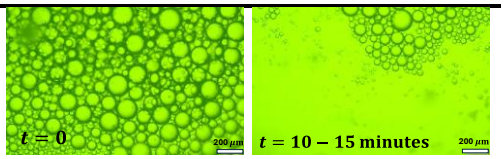
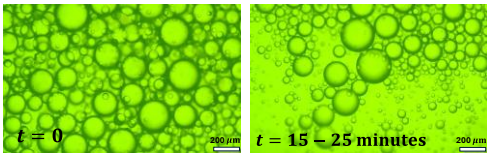
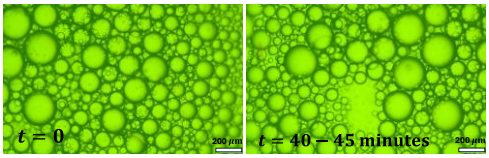
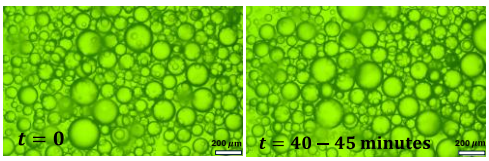
As the XG concentration increases to the range of 0.16-0.2% w/v, emulsion stability dramatically improves. In this range, XG provides sufficient viscosity to minimize droplet mobility and decrease droplet collisions, thereby inhibiting coalescence and separation[27]. The pseudoplastic (shear-thinning) behavior of XG solutions at these concentrations contributes to

their efficacy as emulsion stabilizers[28]. However, at high concentrations (0.24-0.267% w/v), the solution becomes excessively viscous, trapping air bubbles and becoming impractical for further applications. Based on our observations and literature findings, a concentration range of 0.16% to 0.2% w/v of XG in DI water was identified as optimal for maintaining stable emulsions while retaining practical handling properties.

To achieve a good balance between stability and practical handling properties, 0.173% w/v was adopted as the standard concentration throughout our investigation. This concentration provides sufficient viscosity to prevent droplet coalescence while avoiding the practical difficulties associated with higher XG concentrations.

The stabilizing mechanism of XG at the selected concentration can be attributed to its ability to increase the viscosity of the continuous phase, thereby reducing the mobility of emulsion droplets and inhibiting aggregation or coalescence[27].

Table 1: Effect of XG concentration on emulsion stability.

Mass of XG (g) in 7.5 ml DI water	**w/v%**	**Observations**	**Approx. Stability Time**
0.006	0.08	Negligible stability	 10-15 minutes
0.008	0.107	Slight improvement in stability, but oil still separates easily	 15-25 minutes
0.01-0.015	0.133-0.2	Moderate to high stability. Oil dispersion improves significantly; optimal performance	 40-45 minutes
0.018-0.02	0.24-0.267	Solution becomes too thick; air bubbles get trapped and can't escape	

These findings align with literature reports indicating that xanthan gum concentrations between 0.15% and 0.3% are effective for stabilizing various types of emulsions[26,27,29]. The shear-thinning behavior of xanthan gum at the selected concentration provides an additional advantage during the emulsion preparation process, allowing for effective dispersion during mixing while maintaining stability afterward[28].

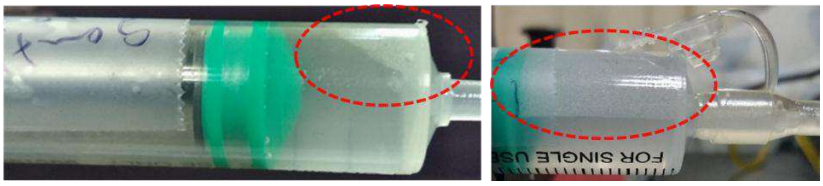


Fig. 2: Rapid droplet coalescence (within 2–5 minutes) in syringes at low XG concentrations (0.08–0.1% w/v), demonstrating poor emulsion stability.

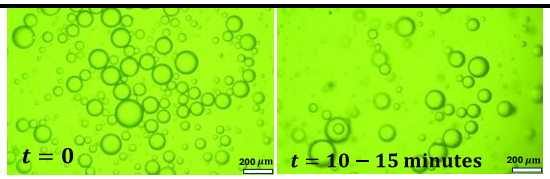
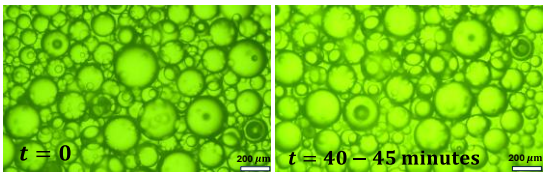
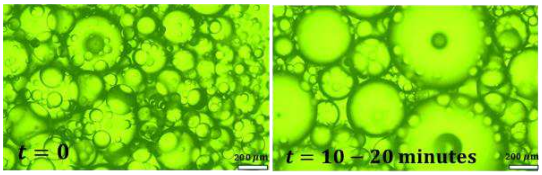
2.1.2 Effect of Mineral Oil Concentration in Emulsion Preparation

Building on the critical role of Xanthan Gum (XG) concentration in stabilizing emulsions, this section investigates how mineral oil concentration further influences emulsion properties. The stability and functionality of the emulsion are critically influenced by the concentration of mineral oil in the XG + DI solution. To evaluate this relationship, mineral oil was added to the solution at varying volumes, resulting in oil-to-solution ratios ranging from 1:30 to 2:5 (Table 2). These ratios were tested at XG concentrations of $0.16 - 0.173\%$ w/v, with observations highlighting the importance of balancing oil content for optimal emulsion performance.

At the lowest oil concentration (1:30 ratio, 0.25 mL oil in 7.5 mL solution), the emulsion exhibited minimal droplet formation and poor stability due to insufficient oil content (Table 2). This instability rendered the emulsion unsuitable for experimental use. Conversely, excessive oil (2:5 ratios, 3.0 mL oil) led to rapid coalescence of droplets during preparation, producing an inhomogeneous emulsion unfit for analysis. Between these extremes, intermediate oil-to-solution ratios (1:15 to 1:4) yielded stable emulsions, with the 1:15 ratio (0.5 mL oil) emerging as optimal for consistent droplet formation and long-term experimental stability (Table 2).

The results, detailed in Table 2, underscore the delicate balance required in mineral oil concentration for effective emulsion preparation. Excessively low or high oil content disrupts emulsion integrity, whereas intermediate ratios enable reliable droplet formation and stability, forming the foundation for studying encapsulated compound droplet dynamics in stenosed geometries.

Table 2: Effect of mineral oil concentrations.

Volume of Oil (mL) in 7.5 ml of Solution	Oil-to-Solution Ratio	Observations at XG concentration (w/v%) of 0.16 and 0.17333
0.25	1:30	 Very low oil concentration; minimal droplet formation and poor stability. (Unstable < 10 min)
0.5 1.0 1.5 2.0 2.5	1:15 2:15 1:5 4:15 1:4	 Ideal for the experiment as the emulsion remains stable for a sufficient period of time. (Stable > 40 min)
3.0	2:5	 Excessive oil; early coalescence of droplets; emulsion unfit for use. (Unstable < 10 min)

In the rest of the study, the outer continuous phase consists of mustard oil, while the primary dispersed phase is the O/W emulsion (consisting of mineral oil as the inner dispersed phase suspended in the XG+DI inner continuous phase). The XG concentration is fixed at 0.173% w/v, and the oil-to-solution ratio is maintained at 1:15 throughout the experiments unless specified otherwise.

2.2 Rheological Characterisation of XG + DI solution

The rheological properties of the xanthan gum solution were characterized through viscosity measurements conducted using a rheometer (Anton Paar MCR 102) at the Smart Machines and Materials Laboratory, Department of Mechanical Engineering, IIT Patna, India. The XG+DI solution exhibited pronounced shear-thinning behaviour[30,31], as demonstrated by the experimental data presented in the log-log plot in Fig. 3.

The viscosity μ as a function of the strain rate $\dot{\gamma}$ is described by the Carreau model equation

$$\mu = \left(\mu_\infty + (\mu_0 - \mu_\infty)[1 + \dot{\gamma}^2\lambda^2]^{(n-1)/2} \right) \quad (1)$$

where, μ_o: zero-shear viscosity, μ_∞: infinite-shear viscosity, n: power-law index, λ: time constant, and $\dot{\gamma}$: shear rate.

The Carreau model[32,33] was chosen as it is a standard and effective empirical model for describing the full shear-thinning flow curve of xanthan gum solutions, accurately capturing both the zero-shear (μ_0) and infinite-shear (μ_∞) plateaus observed in our data.

Fig. 3 illustrates the viscosity profile generated by the Carreau model using the parameters specified in the figure inset. The model parameters were determined through curve-fitting of the experimental data, achieving excellent agreement between the measured and modelled viscosity across the relevant range of strain rates. This rheological characterization is important because understanding the flow behavior of the XG+DI solution is crucial for its effective formulation and application in relevant processes.

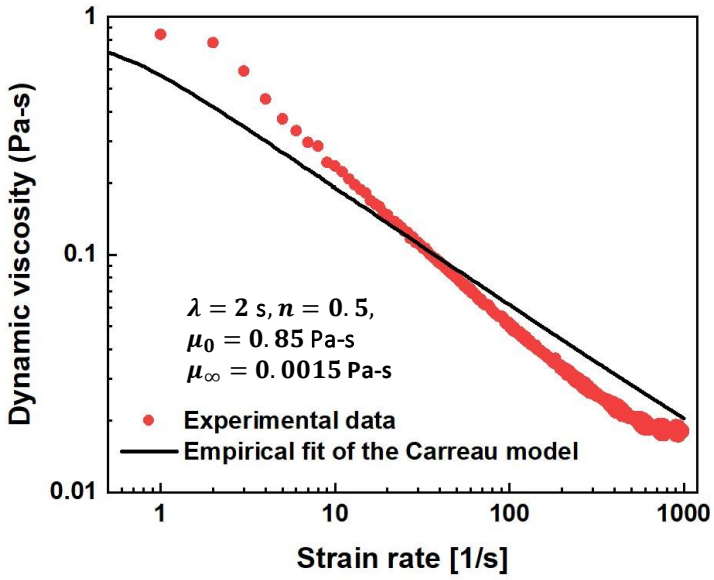


Fig. 3: Experimental and modelled viscosity-strain rate relationship using Carreau model (Eq. 1).

2.3 Microchannel Design

The microchannel geometry and dimensions used in this study are consistent with those described in our previous work [34]. However, to ensure full clarity, we provide the detailed fabrication methodology below.

Rigid-Walled Channel: A 10:1 PDMS-to-curing agent (Sylgard-184) mixture was prepared, cast, and cured to form the PDMS layer. This layer, containing the microchannel, was then irreversibly bonded to a standard 1.5 mm thick glass slide using oxygen plasma, creating a channel with three PDMS walls and one rigid glass bottom[34].

Compliant-Walled Channel: A thin PDMS membrane (10:1 ratio) was prepared separately by spin-coating[35] the PDMS mixture onto a silicon wafer to achieve a final thickness of 0.1318±0.0085 mm. This membrane was cured and carefully peeled. A separate PDMS block containing the microchannel geometry (fabricated as described above) was then bonded to this thin, flexible membrane using oxygen plasma, resulting in a channel with three PDMS walls and one flexible bottom wall.[36] A detailed fabrication steps for both rigid and compliant microchannels have been shown in Fig. B1 (see APPENDIX B).

In this study, a 10:1 ratio was chosen for both rigid and compliant channels to maintain consistency in material properties while focusing on the specific effects of wall compliance.

2.4 Experimental Setup

The experimental setup, illustrated in Fig. 4, consists of two syringe pumps, a microscope, a high-speed camera, a microchannel, and a computer. Droplet motion was analysed using the high-speed camera (Kronos CR14-1.1-32M, Canada), capturing formation, deformation, and transit through the stenosed region. The computer was connected to the camera for better visualisation of the droplet motion.

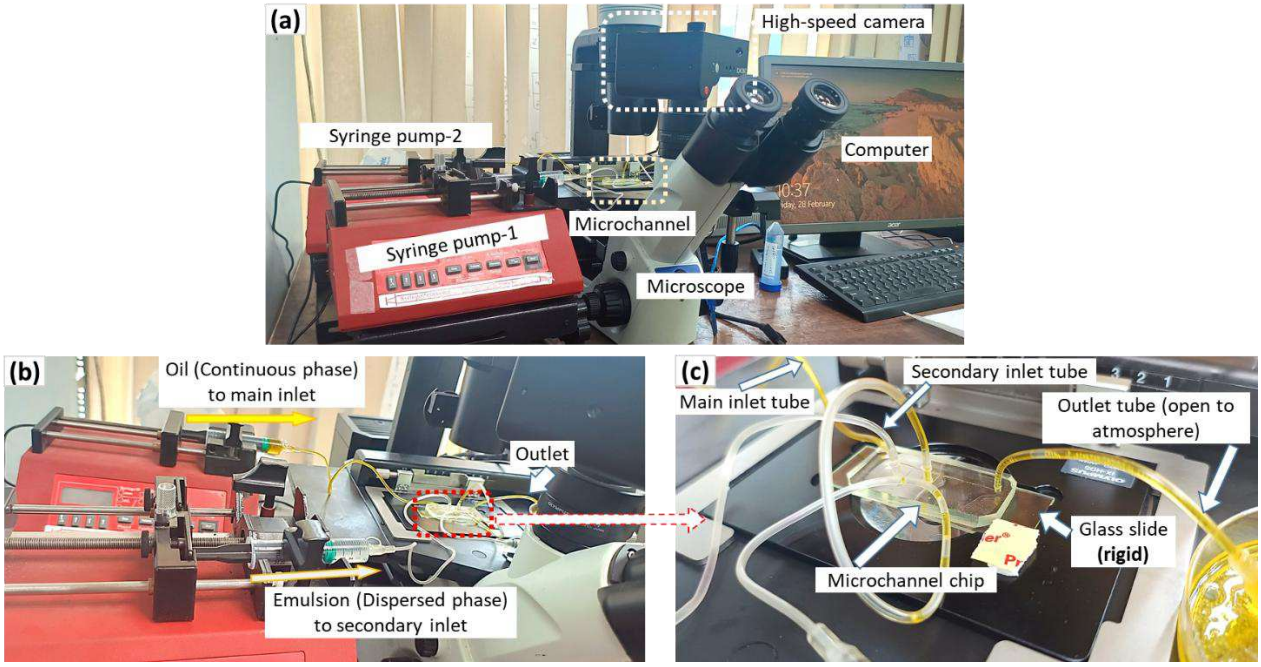


Fig. 4: Experimental setup: (a) overall setup, (b) inlets and outlet tubes, and (c) connections to the microchannel.

The droplet generation process occurs at the T-junction of the microchannel, as illustrated in the schematic in Fig. 5. This setup generates a (O/W)/O multiple emulsion. The primary dispersed phase (the O/W emulsion prepared in Sec. 2.1, consisting of mineral oil droplets as the inner dispersed phase suspended in the XG+DI inner continuous phase) is allowed to pass through the secondary inlet at flow velocity Q_2. The outer continuous phase (mustard oil) is introduced through the main inlet at flow velocity Q_1. The outer continuous phase, flowing at a higher velocity, shears off the primary dispersed phase, resulting in the formation of an emulsion-encapsulated compound droplet. This process enables the controlled generation of droplets for further analysis of their dynamics and behaviour.

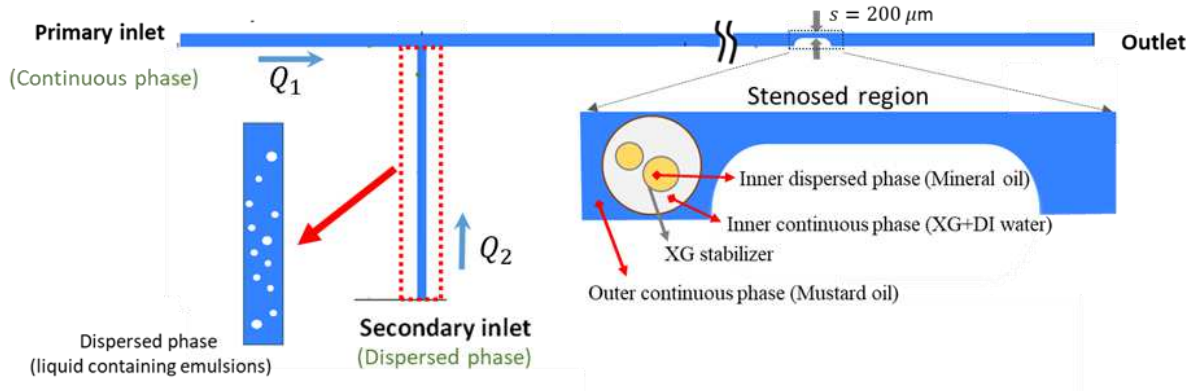


Fig. 5: Schematic of the microchannel with T-junction droplet generator. (Inset) A magnified cartoon labeling the four components of the (O/W)/O multiple emulsion droplet.

3 Results and Discussion

This section examines the influence of key parameters on droplet dynamics and emulsion stability. It begins by analysing the effects of flow rates and the size of droplets on the total transition time of the droplet. The section further explores factors affecting the number of droplets and concludes with a comparative analysis of droplet behaviour in rigid versus compliant-walled channels. In this study, lengths are non-dimensionalised using the stenosis width (s). The outer droplet length (L^*_{od}) and the largest inner droplet diameter ($D^*_{i,max}$) are normalised by the stenosed gap length, where $L^*_{od,avg}$ denotes the average outer droplet length relative to the stenosed gap.

3.1 Effect of Flow Rate Ratio and Size of Inner droplets on Transit Time

A key objective of this study is to understand how the inherent variation in the encapsulated inner droplets, a characteristic of the primary O/W emulsion, which impacts the overall transit dynamics. This variation provided a natural range of inner droplet sizes (e.g., $D^*_{i,max}$ from 0.21 to 1.11). This section leverages this variation to systematically analyze its effect on t_{total}, demonstrating that the internal droplet size is a critical, measurable parameter influencing passage, not an experimental inconsistency. Among the possible descriptors of internal structure, the diameter of the largest encapsulated inner droplet is used here as a representative internal length scale, as it is the most reliably measurable parameter from optical microscopy and exerts a dominant influence on compound droplet deformability under confinement. [14,18] While the inner-phase volume fraction is a more fundamental descriptor of effective viscosity and internal resistance, its quantitative interpretation requires detailed compound-droplet rheological characterisation, which is beyond the scope of the present study.[14,18]

The motion of encapsulated compound droplets is influenced by several factors, including the flow rate ratio ($Q_r = Q_1/Q_2$). As shown in the semi-log plot in Fig. 6a, the average outer droplet length, $L^*_{od,avg}$, shows a strong, near-linear decreasing trend against Q_r when plotted on a logarithmic y-axis, confirming an exponential-like relationship. The analysis is based on 50 data points. This shows that with the increment in the flow rate ratio Q_r, the overall size of the sheared droplet decreases due to the increment in the shearing force. Furthermore, Fig. 6b shows that the total transit time, t_{total}, also follows this strong exponential-like decrease as the flow rate ratio increases, appearing as a near-straight line on this semi-log plot. This can be attributed to the fact that higher flow rate ratios lead to faster movement of the outer droplet,

which in turn reduces the overall time required for the droplet to pass through the stenosed region.

To examine this specific effect, we extracted five cases at $Q_r = 5$, where outer droplets had almost identical sizes but contained inner droplets of varying dimensions (see Fig. 7). This finding is quantitatively demonstrated in the scatter plot in Figure 8, which shows t_{total} as a function of $D^*_{i,max}$. While the data shows a general positive trend, a clear comparison is seen when grouping the data. The first group, with smaller inner droplets ($0.21 \leq D^*_{i,max} \leq 0.25$), has a mean t_{total} of 48.35 ± 0.96 ms. The second group, with larger inner droplets ($0.65 \leq D^*_{i,max} \leq 1.11$), shows a significantly higher mean t_{total} of 52.27±1.03 ms. This visualization confirms the approximately 8% increase in transit time is directly correlated with the size of the encapsulated inner droplets.

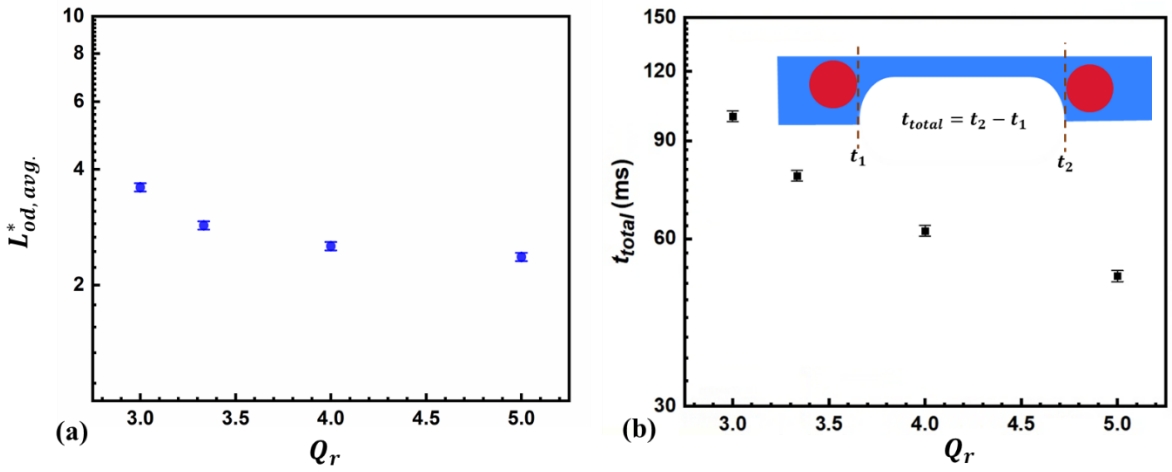


Fig. 6: Effect of flow rate ratio on the (a) outer droplet length and (b) total transit time.

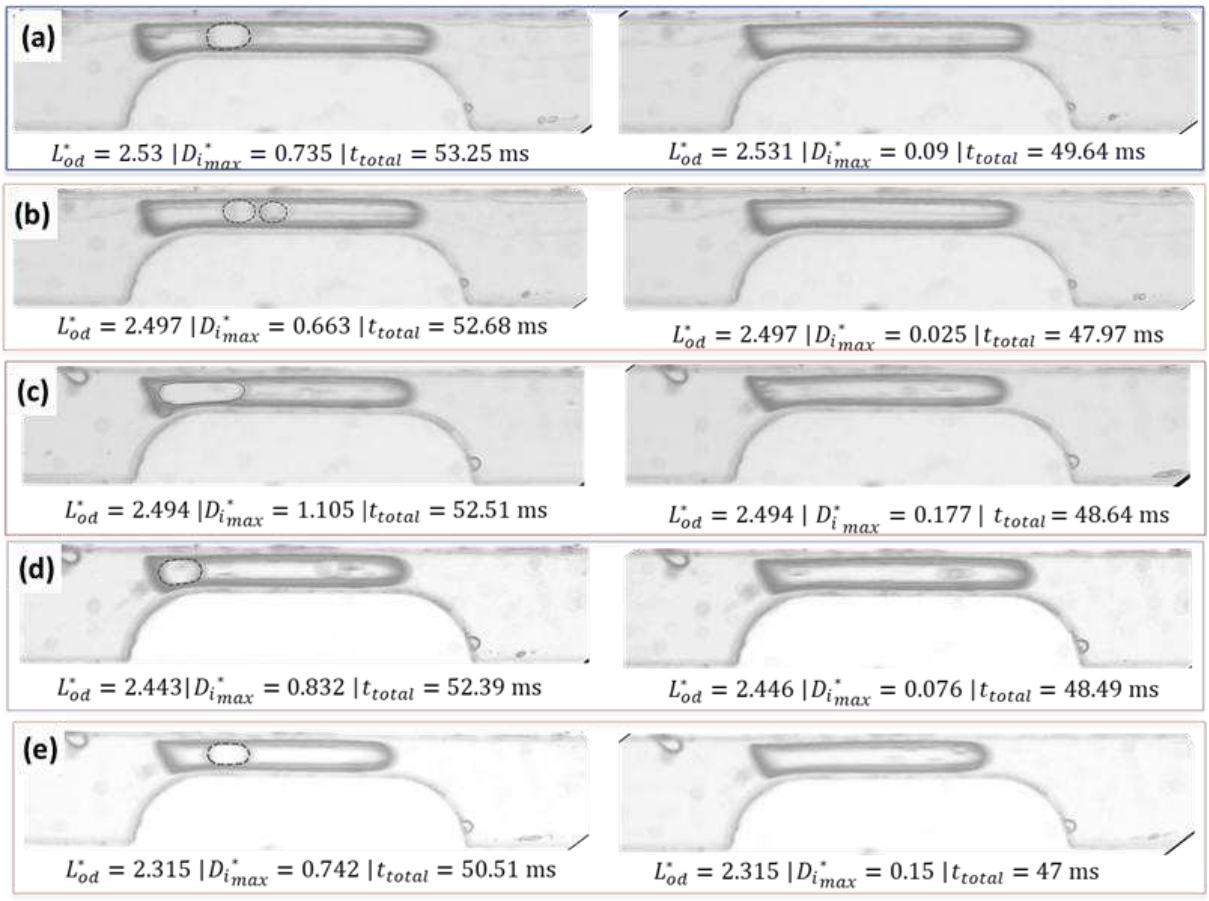


Fig. 7: Comparison of t_{total} for cases with smaller inner droplets ($0.21 \leq D^*_{i,max} \leq 0.25$) against those with larger inner droplets ($0.65 \leq D^*_{i,max} \leq 1.11$) but outer droplets of nearly identical size.

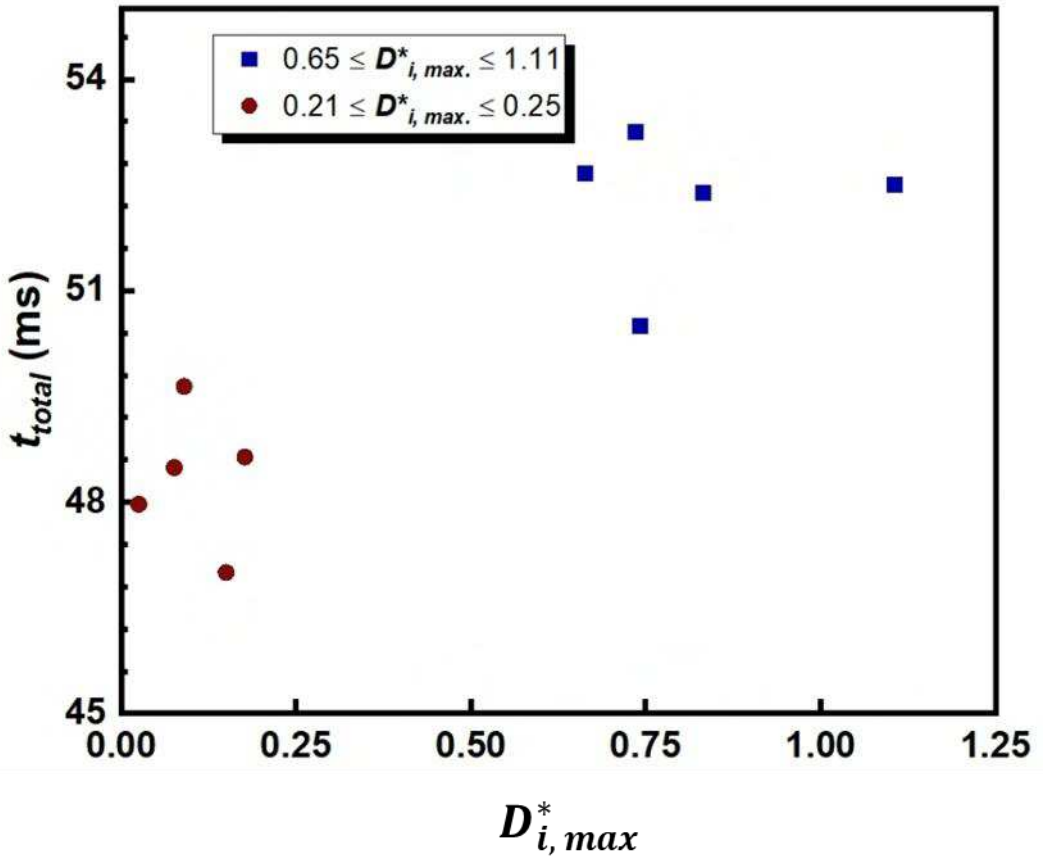


Fig. 8: Quantitative comparison of t_{total} for cases with tiny and larger inner droplets but outer droplets of nearly identical size at $Q_r = 5$. Scatter plot showing the total transit time (t_{total}) as a function of the normalized inner droplet diameter ($D^*_{i,max}$) at $Q_r = 5$. The plot shows a positive correlation, confirming that droplets with larger inner diameters (e.g., $D^*_{i,max} > 0.65$) have a significantly longer transit time compared to those with smaller diameters (e.g., $D^*_{i,max} < 0.25$).

This correlation was confirmed with a paired t-test, conducted to compare the mean total transit time of droplets under two conditions: droplets encapsulating inner droplets $0.65 \leq D^*_{i,max} \leq 1.11$ range (Variable 1) versus those with inner droplets in the $0.21 \leq D^*_{i,max} \leq 0.25$ range (Variable 2), as shown in Table 3. The statistical analysis revealed a highly significant difference in transit times between the two groups, with a t-statistic of 18.57 and a two-tailed p-value of approximately 4.95×10^{-5}, which is far below the conventional significance level of 0.05. This result strongly supports that the presence of larger encapsulated droplets leads to a notably longer transit time through the constricted region, potentially due to increased hydrodynamic

resistance or deformation behavior under confinement. These findings further confirm the impact of internal droplet on droplet dynamics in microfluidic environments.

A direct visual comparison of this phenomenon at $Q_r = 3.333$ is provided in the supplementary video (see Multimedia View[1]), which shows the slower-moving droplet (Case-2, $t_{total} \approx 108.5$ ms) has visibly larger inner droplets than the faster-moving droplet (Case-1, $t_{total} \approx 97.8$ ms).

Table 3: Statistical comparison of droplet transit times with and without large internal droplets using paired t-test.

	Variable 1	*Variable 2*
Mean	52.27	48.35
Variance	1.07	0.93
Observations	5	5
Pearson Correlation	0.89	-
Hypothesized Mean Difference	0	-
df	4	-
t Stat	18.57	-
P($T \leq t$) one-tail	2.47E-05	-
t Critical one-tail	2.13	-
P($T \leq t$) two-tail	4.95E-05	-
t Critical two-tail	2.78	-

Fig. 9 illustrates the effect of inner droplet size ($D^*_{i,max}$), outer droplet size (L^*_{od}), and their ratio ($D^*_{i,max}/L^*_{od}$) on the total transit time (t_{total}) of encapsulated compound droplets through stenosed microchannels. Fig. 9a shows the variation of t_{total} with respect to $D^*_{i,max}$ and L^*_{od}. The results indicate that larger inner droplets lead to increased transit times due to reduced deformability and greater resistance during passage through the constriction. Similarly, larger outer droplets also require more time to traverse the stenosed region, as their increased size interacts more extensively with the channel walls. The influence of the ratio $D^*_{i,max}/L^*_{od}$ on t_{total} is shown in Fig. 9b. A linear fit applied to this data reveals a strong positive correlation ($R^2 = 0.657$), confirming this trend. Higher ratios, indicative of relatively larger inner droplets compared to outer droplets, result in longer transit times. This trend underscores the compounded effect of inner droplet size on the overall dynamics of compound droplets, as larger

[1] https://tinyurl.com/Multimediaview1

inner droplets occupy a significant portion of the outer droplet volume, restricting its ability to deform and adapt to the constricted geometry.

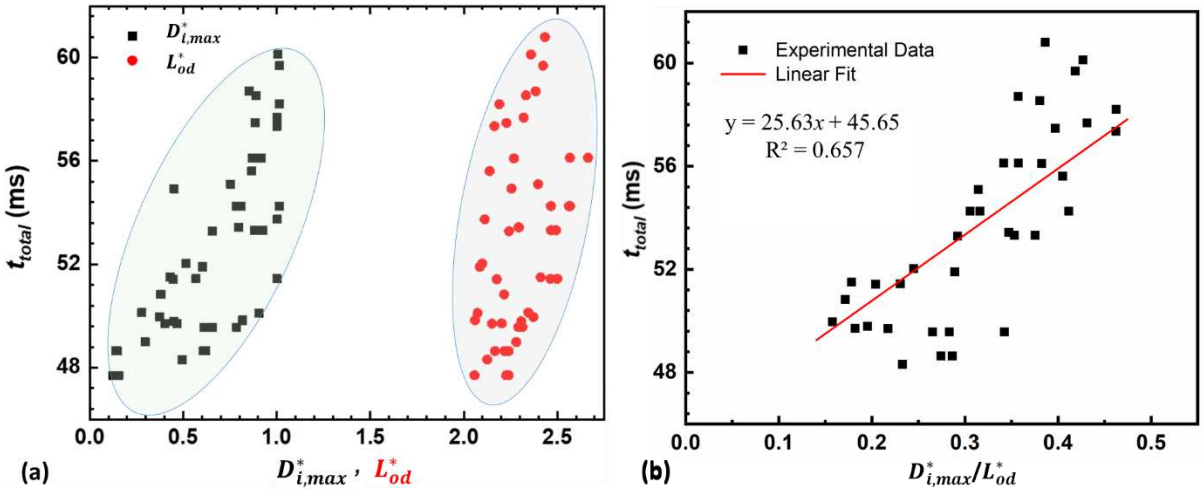


Fig. 9: Effect of inner droplet size ($D^*_{i,max}$) and outer droplet size (L^*_{od}) on the total time t_{total} at $Q_r = 5$; (a) variation of t_{total} with respect to $D^*_{i,max}$ and L^*_{od}, (b) influence of the ratio $D^*_{i,max}/L^*_{od}$ on t_{total}, showing a positive linear correlation ($R^2 = 0.657$).

The observed increase in transit time with larger inner droplets can be attributed to both reduced deformability of the compound droplet system and the complex rheological interactions between the encapsulated mineral oil and the xanthan gum solution. When larger inner oil droplets are present, they occupy a substantial portion of the outer droplet volume, restricting the ability of the compound structure to deform as it navigates through the stenosed region. Additionally, the viscosity contrast between the mineral oil (Newtonian fluid) and the xanthan gum solution (shear-thinning non-Newtonian fluid) creates complex flow patterns within the encapsulated compound droplet.

The shear-thinning nature of the xanthan gum solution means its viscosity decreases under higher shear rates [30,31], which occur most prominently at the stenosed region. With larger encapsulated oil droplets, the effective viscosity distribution within the compound droplet changes, potentially leading to altered flow characteristics and increased resistance as the droplet moves through the constriction. This rheological complexity, combined with the reduced deformability, explains the longer transit times observed for droplets containing larger inner oil phases despite having similar outer dimensions.

3.2 Factors Influencing the Number of Encapsulated Droplets

While Section 3.1 analyzed the effect of a polydisperse inner droplet population on transit time, this section briefly discusses the parameters that control the encapsulation process itself. Building on the interplay of XG concentration (Section 1.1.1), mineral oil concentration (Section 1.1.2), and flow rate ratios (Section 2.1), this section examines how these parameters collectively influence the characteristics of the encapsulated droplets (e.g., outer droplet size and the number of inner droplets). To clarify, our primary measured variable was the size of the largest inner droplet ($D^*_{i,max}$), as this had the most significant and reliably measurable impact on transit dynamics, rather than the total count of inner droplets, which was more variable. The formation and stability of these (O/W)/O multiple emulsion droplets depend on a balance of hydrodynamic forces and material properties, as summarized in Table 4.

Table 4: Factors influencing encapsulated droplets.

Parameters	Reason
Flow Rate Ratio (Q_r)	The size of the outer droplet is directly influenced by the flow rate ratio (Q_r) at fixed concentration of XG and oil. A lower Q_r typically results in larger outer droplets, which can encapsulate more inner droplets. Conversely, a higher Q_r produces smaller outer droplets, limiting the number of encapsulated droplets.
XG Concentration	The concentration of Xanthan Gum (XG) in the XG+DI solution determines the stability of the solution. Higher XG concentrations increase viscosity and improve droplet stability, enabling better encapsulation. However, excessively high XG concentrations can lead to increased viscosity, making droplet formation difficult.
Oil Concentration	The concentration of oil in the emulsion affects the number of droplets available for encapsulation. Increasing the oil concentration enhances the density of droplets in the emulsion, potentially increasing the number of encapsulated droplets. However, too much oil can lead to coalescence, reducing the stability of the emulsion and the uniformity of encapsulation.

This analysis integrates material, hydrodynamic, and geometric parameters to provide a framework for tailoring multiple emulsion droplet systems in microfluidic applications.

3.3 Comparison between Rigid and Compliant Walled Channels

The mechanical properties of microchannel walls significantly impact droplet generation and transport, particularly when navigating through stenosed regions. To investigate this, we compared the two channel configurations fabricated in Section 2.3: the rigid-walled (PDMS-on-glass) channel and the compliant-walled (PDMS-on-membrane) channel.

We acknowledge that the compliance is qualitative (i.e., inferred from the known material properties and the significant difference in wall thickness) and not directly quantified. The focus of this study is on the measurable effects of this known compliance on the droplet's transit dynamics. This investigation builds upon our earlier findings from single droplet analysis, where wall compliance was shown to significantly influence droplet dynamics, including droplet entry and passage times. The current study extends these observations to encapsulated compound droplets, providing further insights into the role of wall compliance in complex droplet systems.

3.3.1 Effect on Droplet Generation Point

In the compliant-walled channel, encapsulated droplets consistently formed at or near the secondary inlet's T-junction (multimedia view[2]). This observation of early onset droplet generation in compliant channels aligns with the findings reported by Raj et al.[37], who explored the impact of wall compliance on droplet mobility through deformable, non-stenosed microchannels. Their work underscored the significance of wall deformability in altering droplet formation dynamics and location.

In contrast, in the rigid-walled channel, droplets originated farther downstream, typically more than halfway between the secondary inlet and the stenosed region (multimedia view[2]). The rigid walls maintain consistent channel geometry regardless of flow conditions, resulting in different droplet formation dynamics compared to the compliant channel.

This difference in droplet generation location can be attributed to the deformability of the compliant wall, which creates a dynamic coupling between fluid flow and channel geometry. As demonstrated in comprehensive investigation by[37], the bulging effect caused by fluid-structure interactions between the internal viscous flow and the soft walls alters the effective

[2] https://tinyurl.com/multimediaview03

channel geometry, particularly at the junctions, resulting in different pressure gradients and flow patterns compared to rigid channels.

3.3.2 Effect on Total Transit Time

Under the same size ratio of $D^*_{i,max}/L^*_{od}$, t_{total} is plotted for four different flow rates within range $3 \leq Q_r \leq 5$ for rigid and compliant as shown in Fig. 10. It can be observed that at a particular flow rate ratio, the t_{total} was higher in the compliant-walled channel compared to the rigid-walled channel. To have a better comparison, a box plot is prepared and shown in Fig. 11, which compares t_{total} in rigid and compliant stenosed channels under the same size of inner and outer droplets. It is to be noted here that the t_{total} here is the average total transit time taken by the droplets to cross the stenosed region. It can be observed that the maximum increase in t_{total} is 35.07% in the compliant channel compared to the rigid channel at $Q_r = 3.333$, while the minimum increase is 24.17% at $Q_r = 5$, as depicted in Fig. 11.

This passage of a droplet through a narrow constriction is fundamentally governed by the formation of a thin lubrication film between the droplet and the channel wall, a phenomenon first described by Bretherton[17]. In this classical framework, the pressure drops required to propel the droplet is highly sensitive to this film's thickness. Our results suggest this framework is modulated by wall compliance.

This increased transit time in compliant channels can be attributed to the dynamic coupling between fluid flow and channel geometry created by wall deformation. As the encapsulated compound droplet approaches the stenosed region, the pressure increases, causing the compliant membrane to deform outward further. This deformation creates a curved surface that alters the contact angle distribution along the droplet interface, resulting in increased resistance to motion[34]. This finding is consistent with our previous work[34] where the curvature effect has throttled the droplet motion and led to longer entry and passage times. Furthermore, as established by Raj et al.[37], the compliant wall absorbs excess hydrodynamic stress from the droplet interface during transit. This stress absorption effectively dissipates a portion of the driving energy that would otherwise propel the droplet, thereby altering the migration dynamics and leading to the observed increase in transit time compared to the rigid channel.

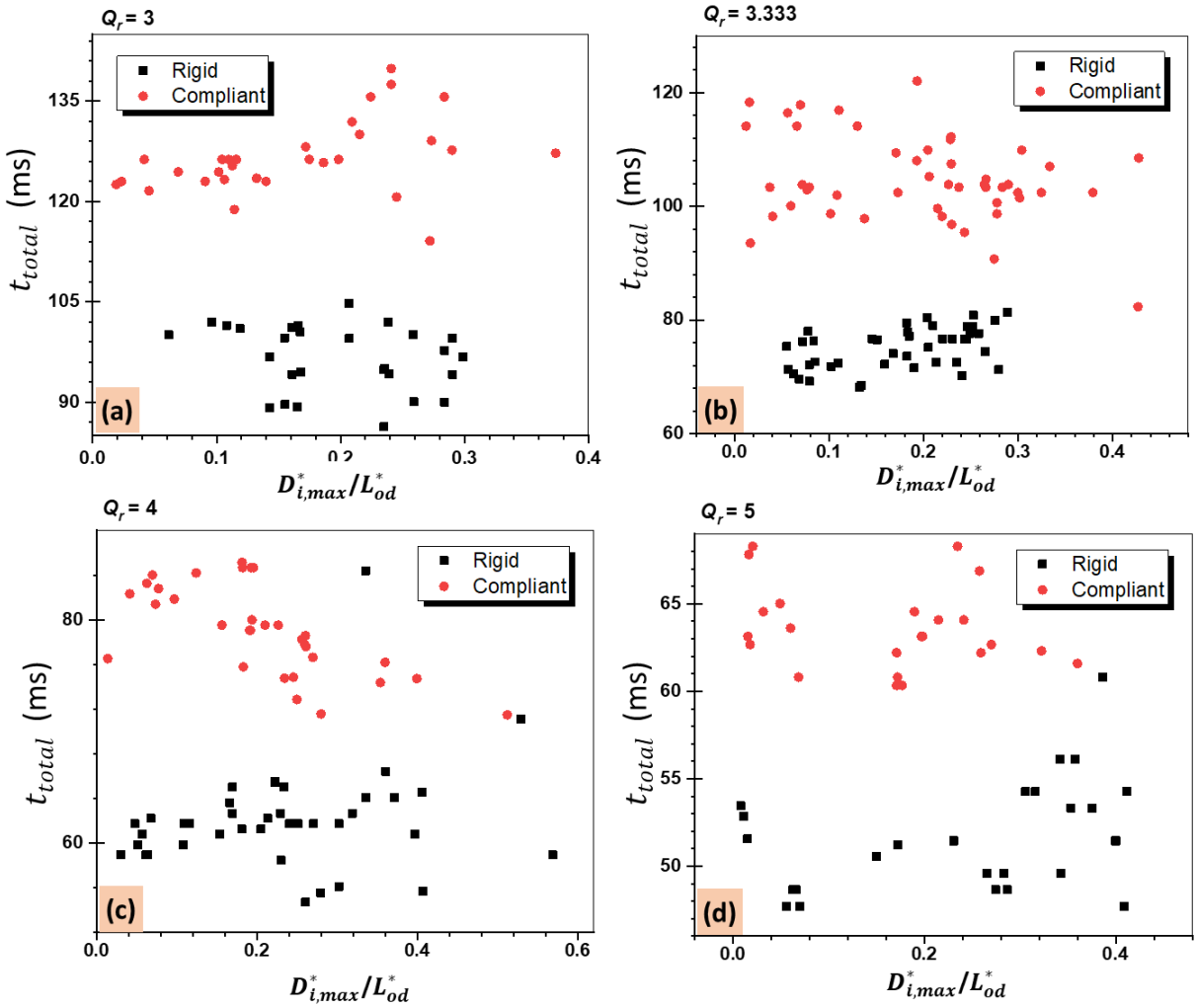
Unlike the case of single cells in microchannels, where Raj and Sen [37,38] reported decreased entry times with increased wall compliance, our compound droplets experience a different behaviour. This difference likely comes from the unique nature of encapsulated compound droplets, where inner droplets contribute to the overall resistance to deformation of the entire

structure. The curved deformation of the compliant wall creates a non-uniform confinement geometry that restricts the ability of the compound droplet to adapt its shape during passage, particularly when large inner droplets are present.

Additionally, in highly compliant microchannels, the wall expansion can temporarily store fluid and reduce hydraulic resistance. While this might suggest faster transit, it also means that more complex pressure distributions develop around the compound droplet. The deformed membrane creates a scenario where the droplet must navigate a dynamically changing environment, effectively increasing the functional length of the stenosed region from the droplet's perspective.

While droplet length could theoretically influence transit time, it was not the primary factor in this study. The consistent trend of higher transit times in compliant channels across all tested flow rate ratios ($3 \leq Q_r \leq 5$) indicates that this is a fundamental characteristic of encapsulated compound droplet behaviour in deformable stenosed microchannels rather than a flow-rate dependent phenomenon. This consistency suggests that the geometric effects of wall deformation dominate over potential benefits from reduced hydraulic resistance, particularly in the complex case of encapsulated compound droplets navigating through constrictions.

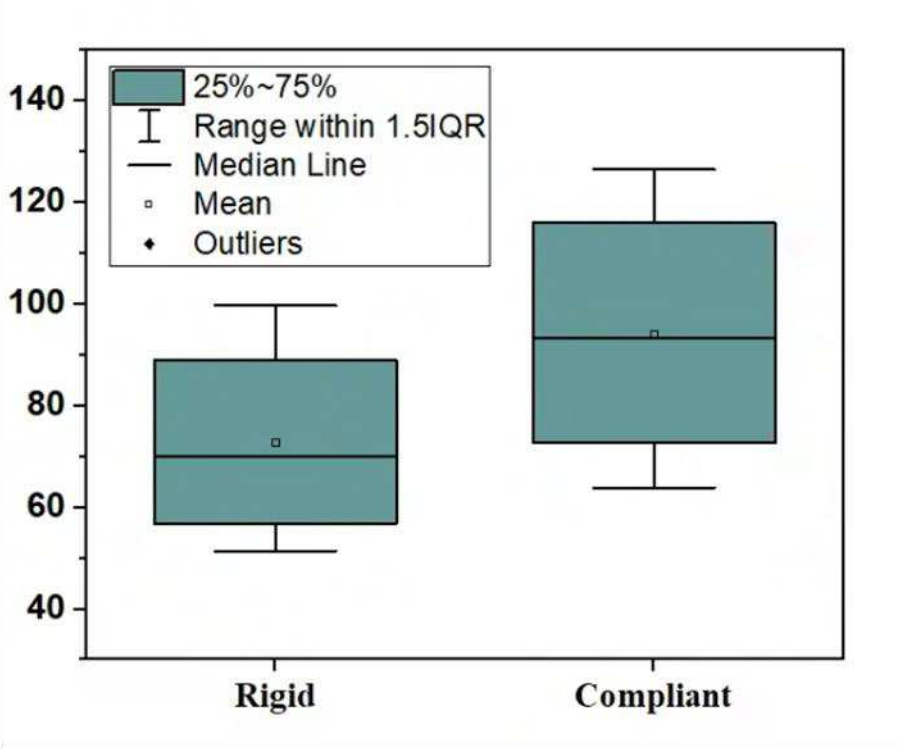
While our current investigation provides valuable insights into the impact of wall compliance on transit time, future extensions of this work could incorporate direct measurement and quantification of wall deformation during droplet passage. Advanced imaging techniques such as confocal microscopy or interferometric methods, similar to those employed by Raj et al.[37], could be implemented to precisely map the membrane deformation profile at various flow conditions. Such measurements would allow for better quantification of the curvature effect and establish more robust correlations between wall deformation magnitude and the resulting increase in transit time. Additionally, computational fluid-structure interaction modelling could validate experimental observations while offering deeper insights into the local pressure distribution and contact mechanics at the droplet-wall interface.



508

509 Fig. 10: Variation of t_{total} (shown on the vertical axis) with flow rate ratio ($3 \leq Qr \leq 5$) under the same
510 size ratio ($D^*_{i,max}/L^*_{od}$, shown on the horizontal axis), showing higher t_{total} for the compliant channel
511 compared to the rigid channel.

512



$$0.1 \pm 0.001 \leq D^*_{i,max} \leq 1.5 \pm 0.003$$

$$1.53 \pm 0.003 \leq L^*_{od} \leq 3.61 \pm 0.0035$$

Fig. 11: Comparing t_{total} in rigid and compliant stenosed channels under the same size of inner and outer droplets. It is to be noted here that the t_{total} here is the average total transit time taken by the droplets to cross the stenosed region. The plot displays the full statistical range, including the median, mean, and interquartile range.

The results presented here focus on the fluid-mechanical consequences of wall compliance, namely the significant increase in t_{total} (Fig. 11) and the shift in the droplet generation point (Fig. 4). This increased transit time is attributed to the curvature-induced resistance from the deformed membrane, which arises because the compliant wall absorbs the excess mechanical stress exerted by the droplet, thereby altering the migration dynamics as established in previous microchannel studies[39,40]. This absorption of stress alters the hydrodynamic pressure and lubrication film dynamics near the constriction.

The significant variations in transit time observed between rigid and compliant channels have direct implications for microfluidic chemical processing. In applications such as droplet-based micro-reactors, the increased residence time in compliant channels acts as a passive method to extend reaction windows. Conversely, the differential velocities induced by internal droplet size variation could lead to a broadening of residence time distributions, a critical factor that may necessitate tighter upstream control of inner droplet size for sensitive chemical assays.

A precise quantification of the membrane's dynamic deformation profile, while not the primary focus of this study, presents a valuable avenue for future work and would require advanced imaging techniques such as confocal microscopy or interferometry. Similarly, a detailed investigation into how these altered flow patterns influence local chemical behaviors (e.g., mass transfer) would be an important extension, requiring further chemo-mechanical modelling.

4 Conclusion

This study focused on the analysis of emulsion-encapsulated compound droplets navigating through stenosed microchannels, investigating the effects of flow dynamics, material properties, and channel geometry (rigid and deformable wall) on droplet behaviour. The findings highlight several critical aspects:

i. The size and transit time of compound droplets were found to vary exponentially with flow rate ratio, providing insights into optimizing flow conditions for generating monodisperse droplets.

ii. This work introduces a unique method for preparing mineral oil emulsions using an XG+DI solution, ensuring improved emulsion stability and controlled droplet encapsulation. Concentrations in the range of 0.16–0.2% (w/v) provided a good balance between stability and viscosity, ensuring consistent droplet behaviour without significantly altering transit time.

iii. Intermediate oil concentrations (~15% v/v) yielded optimal emulsion stability, while extreme concentrations led to destabilization due to changes in interfacial tension and viscosity.

iv. The number of encapsulated droplets was found to depend on flow rate ratio, XG concentration, and oil concentration. Lower flow rate ratios produced larger outer droplets capable of encapsulating more inner droplets, while optimal XG and oil concentrations ensured stable emulsions that facilitated controlled encapsulation.

v. Wall compliance significantly alters droplet behaviour, leading to earlier droplet formation and consistently longer transit times due to curvature effects from wall deformation. As shown in previous work[34], curvature-induced resistance opposes droplet motion, increasing hydrodynamic resistance and entry and passage time. Similarly, in this study, compliant channels exhibited longer transit times than rigid ones due to curvature-induced hindrance. The maximum percentage increase in t_{total} is observed to be 35.07% in the compliant channel compared to the rigid channel at $Q_r = 3.333$, while

the minimum increase is 24.17% at $Q_r = 5$. The deformation of the compliant wall under pressure modified the effective channel geometry, creating a dynamic coupling between fluid flow and wall elasticity. This interaction not only affected droplet transit but also shifted droplet generation locations near the secondary inlet.

Furthermore, by providing precise fluid-mechanical control over droplet formation and encapsulation, this work offers a foundational method for advancing chemical science applications such as the fabrication of bespoke reactors[41] or multi-layered carriers for controlled release[42].

Collectively, these findings highlight the crucial role of wall compliance and curvature effects in microfluidic droplet dynamics. While previous studies focused on single droplets and their blockage potential, this chapter expands the understanding by examining encapsulated compound droplet behaviour. This work provides important fundamental insights for designing such systems. For example, our quantification of the ≈ 8% increase in transit time for droplets with larger inner cores (i.e., the 'payload') and the maximum 35.07% increase in t_{total} from wall compliance are critical design parameters. These parameters can be directly used to feed input to future computational models, in vitro models of stenosed vessels, or experimental case studies in targeted drug delivery. For instance, accurate prediction of transit time is essential for assessing hemodynamic clearance rates and minimizing the risk of capillary occlusion (embolism) by larger drug carriers[43], and it is crucial for optimizing the residence time distribution in micro-reactors to ensure uniform reaction yields[44].

Future research should focus on quantifying wall deformation effects and incorporating adaptive meshing techniques to simulate more complex emulsion systems. Future studies should also focus on quantifying other key dimensionless parameters, such as the internal volume fraction of the inner dispersed phase and the total internal interfacial area, which likely play a significant role in the system's bulk rheology and transit dynamics. This should be coupled with a more detailed rheological characterization, including oscillatory measurements and analysis of the individual fluid components, to build a more comprehensive chemo-rheological model. Additionally, direct measurement of the dynamic wall deformation profiles using techniques like high-speed confocal microscopy or interferometry would provide deeper quantitative insights into the fluid-structure interaction. This work establishes a foundation for advancing microfluidic technologies in biomedical and industrial applications.

Data availability: Data will be made available on request.

Conflict of interest

The authors declare that there is no conflict of interest.

Funding Declaration and Acknowledgement

The author A.R. acknowledges Indian Council of Medical Research (ICMR), Government of India, New Delhi for the financial support under Grant no. 2022-18202/F1. The author A.A. acknowledges the Department of Science and Technology, Government of India, for the financial support under Grant No. DST/INSPIRE/04/2019/001001.

Appendix A: Foamability and Stability of Oil Emulsions Over Time: Comparison of Xanthan Gum (XG), Tween 80, and Span 80.

This appendix compares the foamability and stability of mineral oil emulsions prepared using three different agents: xanthan gum (XG), Tween 80, and Span 80. The results are presented in Figures A1–A3, showing the emulsions at three time intervals: immediately after preparation (t = 0), 1 hour, and 12 hours. Each figure includes three subfigures: (a) emulsion with XG, (b) emulsion with Tween 80, and (c) emulsion with Span 80.

The mineral oil emulsion prepared with xanthan gum (XG) demonstrates exceptional stability and clarity. Figures A1a, A2a, and A3a show that the emulsion remains stable and transparent even after 12 hours, with almost no foam formation. This makes XG-based emulsions highly suitable for applications requiring experimental stability and optical clarity, such as microfluidic experiments where visibility is critical.

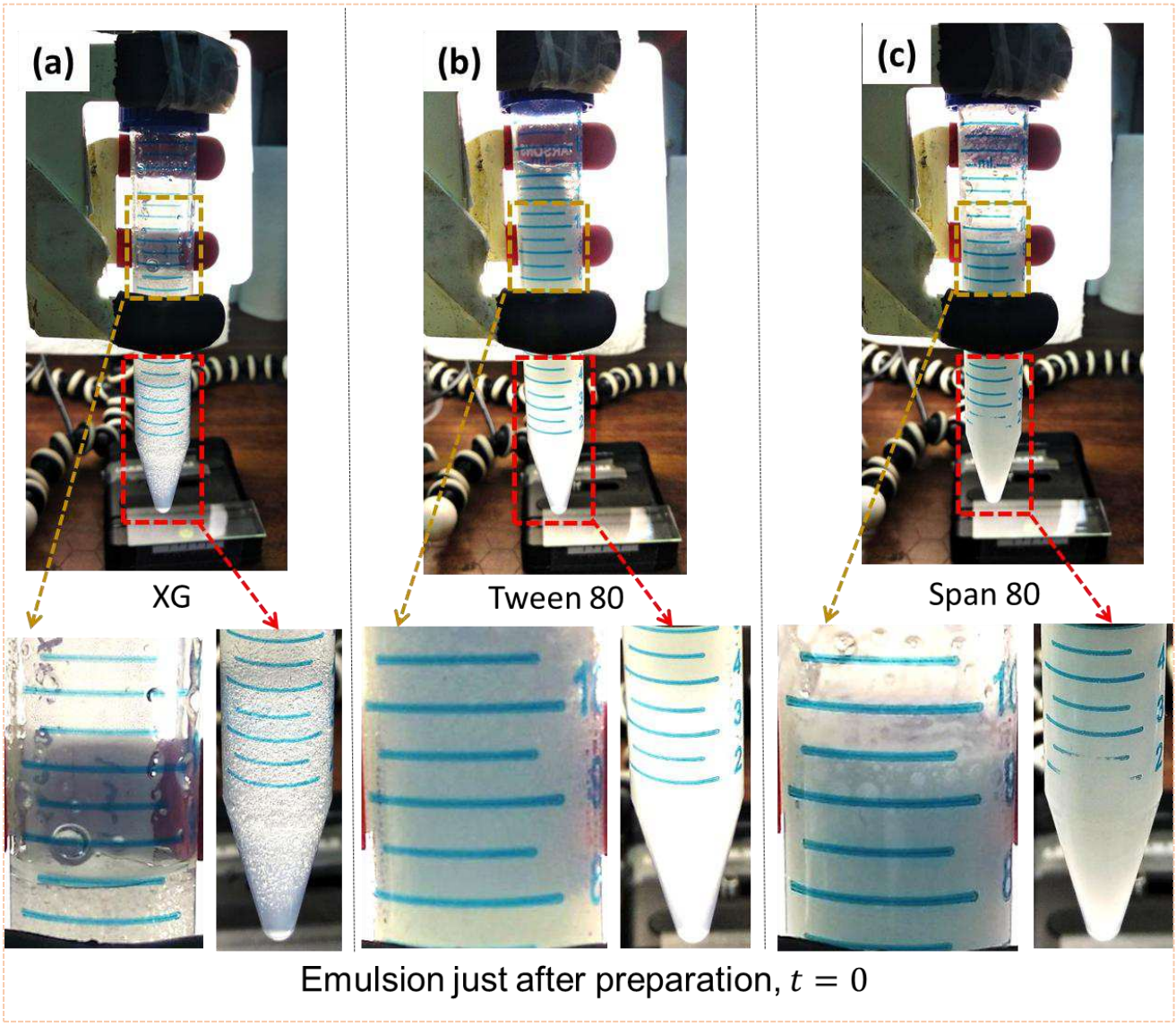
In contrast, the emulsion prepared with Tween 80 shows significant foam formation immediately after preparation (Fig. A1b). Over time, the foam persists, and the mineral oil begins to separate, rising to the surface (Fig. A3b). This indicates poor emulsion stability, which limits its usability in applications where consistent emulsion properties are required. The presence of foam and oil separation also makes it less ideal for experiments requiring clear visual observation.

The emulsion prepared with Span 80 exhibits a different behaviour. Immediately after preparation, it forms a milky white substance (Fig. A1c), which remains unchanged over time (Figs. A2c and A3c). This opacity significantly affects the emulsion's visibility, making it unsuitable for applications where optical clarity is essential. While the emulsion does not

628 separate like the Tween 80-based emulsion, its milky appearance restricts its usability in many
629 experimental setups.

630 The primary advantage of the XG+DI method over traditional surfactants, as shown in
631 Appendix A, is its ability to produce stable, foam-free emulsions with high optical clarity. This
632 was a critical prerequisite for the optical-based analysis of droplet dynamics presented herein,
633 as the foam and opacity from Tween 80 and Span 80, respectively, made visualization very
634 unclear.

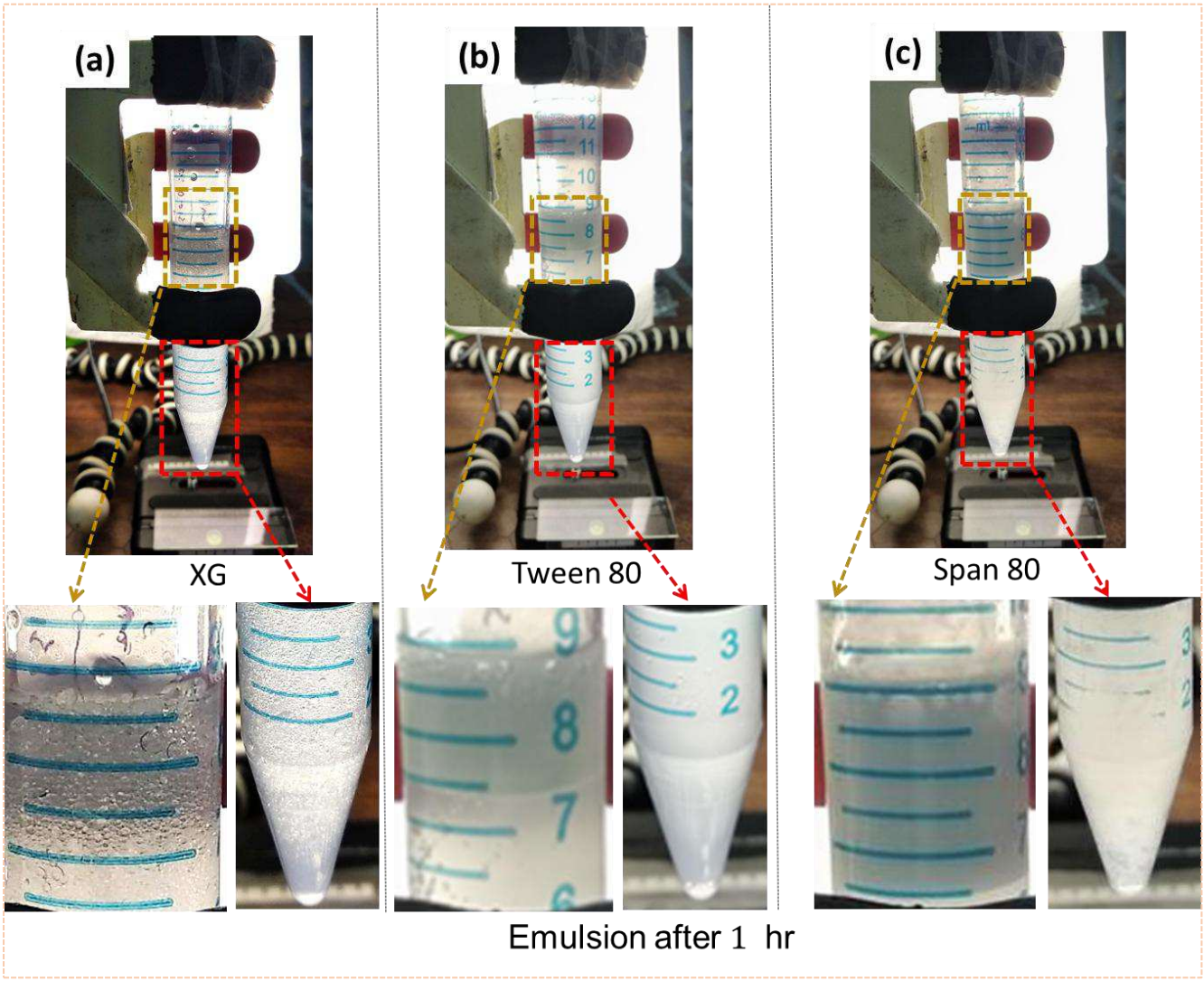
635 The XG-based emulsion demonstrated high stability and optical clarity over a 12-hour
636 period (Fig. A3), which was more than sufficient to ensure consistent properties during all
637 experimental runs. We do not make claims of long-term (e.g., weeks or months) stability. These
638 findings highlight the advantages of using xanthan gum for preparing stable, foam-free, and
639 optically clear emulsions, particularly in microfluidic and other experimental applications where
640 these properties are critical. Hence, it was chosen in the current study.



641

642 Fig. A1. Emulsion just after preparation: (a) with xanthan gum (XG), (b) with Tween 80, and

643 (c) with Span 80.



644

645 Fig. A2. Emulsion stability after 1 hour of preparation: (a) with xanthan gum (XG), (b) with
646 Tween 80, and (c) with Span 80.

647

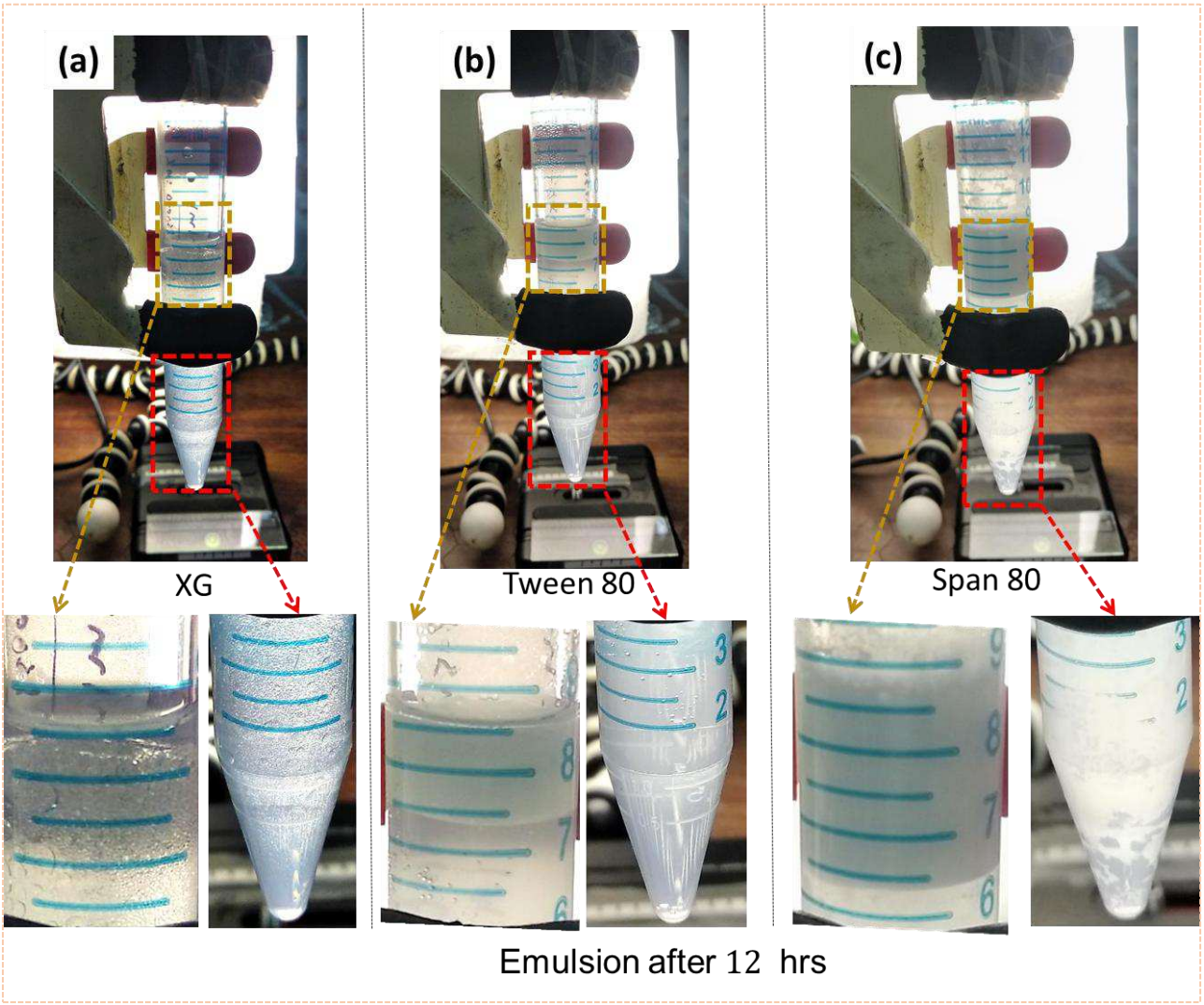


Fig. A3. Emulsion stability after 12 hours of preparation: (a) with xanthan gum (XG), (b) with Tween 80, and (c) with Span 80.

Appendix B: Fabrication of Rigid and Compliant Microchannels

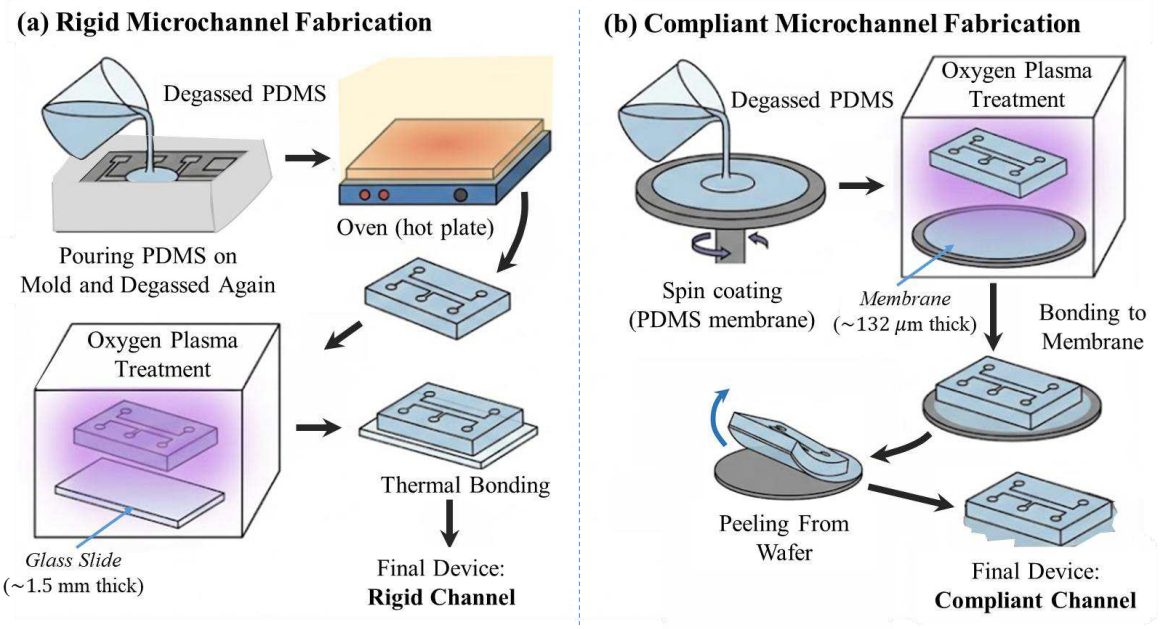


Fig. B1. Fabrication steps for (a) rigid (channel bonded to a glass slide) and (b) compliant (channel bonded to a thin PDMS membrane) microchannels.

References

[1] Z. Li, C. Guo, and Z. Jian, "Compound Droplet Generation by a Hybrid Microfluidic Device," Langmuir, (2024).

[2] H.D. Nguyen, T. V. Vu, P.H. Nguyen, B.D. Pham, N.X. Ho, C.T. Nguyen, and V.T. Nguyen, "Numerical study of the indentation formation of a compound droplet in a constriction," J. Mech. Sci. Technol. **35**(4), 1515–1526 (2021).

[3] M. Damak, J. de Ruiter, S. Panat, and K.K. Varanasi, "Dynamics of an impacting emulsion droplet," Sci. Adv. **8**(11), 1–9 (2022).

[4] P. Kumar, A. Phukan, A. Kumar, M. Pathak, and V. Kumar, "Deciphering the multifaceted impact of nanoparticle concentration on droplet generation dynamics within microfluidic systems," J. Mol. Liq. **412**, 125807 (2024).

[5] A. Sattari, N. Tasnim, P. Hanafizadeh, and M. Hoorfar, "Motion and deformation of migrating compound droplets in shear-thinning fluids in a microcapillary tube," Phys. Fluids **33**(5), (2021).

[6] H. V. Vu, T. V. Vu, B.D. Pham, H.D. Nguyen, V.T. Nguyen, H.T. Phan, and C.T. Nguyen, "Deformation of a compound droplet in a wavy constricted channel," J. Mech. Sci. Technol. **37**(1), 191–202 (2023).

[7] M.A. Hashem, A. Aghilinejad, X. Chen, and H. Tan, "Compound droplet modeling for circulating tumor cell microfiltration with adaptive meshing refinement," J. Fluids Eng. Trans. ASME **142**(11), 1–14 (2020).

[8] S.A. Vagner, and S.A. Patlazhan, "Flow-induced transition of compound droplet to composite

microfiber in a channel with sudden contraction," Phys. Fluids **35**(3), (2023).

[9] N.X. Ho, V.T. Nguyen, H.D. Nguyen, and T. V. Vu, "Dynamics of a compound droplet in a microchannel containing a long obstacle," Eur. J. Mech. - B/Fluids **110**, 25–33 (2025).

[10] D. Wang, F. Serracino-Inglott, and J. Feng, "Numerical simulations of patient-specific models with multiple plaques in human peripheral artery: a fluid-structure interaction analysis," Biomech. Model. Mechanobiol. **20**(1), 255–265 (2021).

[11] Y. Ren, Y. Huang, C. Xie, Y. Yan, J. Wang, and T. Yamaguchi, "Thermal Effect on Deformation of Nanofluid-Encapsulated Double Emulsion Droplets Flowing in a Constricted Microchannel," Heat Transf. Eng. **43**(13), 1135–1148 (2022).

[12] N.X. Ho, H. V. Vu, and T. V. Vu, "Migration of a multi-core compound droplet in a ratchet microchannel," Eur. J. Mech. B/Fluids **105**(February), 285–294 (2024).

[13] C.T. Nguyen, H. V. Vu, T. V. Vu, T. V. Truong, N.X. Ho, B.D. Pham, H.D. Nguyen, and V.T. Nguyen, "Numerical analysis of deformation and breakup of a compound droplet in microchannels," Eur. J. Mech. B/Fluids **88**, 135–147 (2021).

[14] F.Y. Leong, Q. Li, C.T. Lim, and K.H. Chiam, "Modeling cell entry into a micro-channel," Biomech. Model. Mechanobiol. **10**(5), 755–766 (2011).

[15] Z. Che, Y.F. Yap, and T. Wang, "Flow structure of compound droplets moving in microchannels," Phys. Fluids **30**(1), (2018).

[16] J. Gounley, E.W. Draeger, and A. Randles, "Numerical simulation of a compound capsule in a constricted microchannel," Procedia Comput. Sci. **108**, 175–184 (2017).

[17] F.P. Bretherton, "The motion of long bubbles in tubes," J. Fluid Mech. **10**(2), 166–188 (1961).

[18] A. Sattari, N. Tasnim, P. Hanafizadeh, and M. Hoorfar, "Motion and deformation of migrating compound droplets in shear-thinning fluids in a microcapillary tube," Phys. Fluids **33**(5), (2021).

[19] L.A. Bawazer, C.S. McNally, C.J. Empson, W.J. Marchant, T.P. Comyn, X. Niu, S. Cho, M.J. Mcpherson, B.P. Binks, A. Demello, and F.C. Meldrum, "Combinatorial microfluidic droplet engineering for biomimetic material synthesis," Sci. Adv. **2**(10), 1–12 (2016).

[20] T.S. Kaminski, and P. Garstecki, "Controlled droplet microfluidic systems for multistep chemical and biological assays," Chem. Soc. Rev. **46**(20), 6210–6226 (2017).

[21] H. Song, D.L. Chen, and R.F. Ismagilov, "Reactions in droplets in microfluidic channels," Angew. Chemie - Int. Ed. **45**(44), 7336–7356 (2006).

[22] H. Huang, Y. Tian, X. Bai, Y. Cao, and Z. Fu, "Influence of the Emulsifier Sodium Caseinate–Xanthan Gum Complex on Emulsions: Stability and Digestive Properties," Molecules **28**(14), (2023).

[23] M. HENNOCK, R.R. RAHALKAR, and P. RICHMOND, "Effect of Xanthan Gum Upon the Rheology and Stability of Oil-Water Emulsions," J. Food Sci. **49**(5), 1271–1274 (1984).

[24] V. Krstonošić, L. Dokić, I. Nikolić, and M. Milanović, "Influence of xanthan gum on oil-in-water emulsion characteristics stabilized by OSA starch," Food Hydrocoll. **45**, 9–17 (2015).

[25] A. Drakos, and V. Kiosseoglou, "Stability of acidic egg white protein emulsions containing xanthan gum," J. Agric. Food Chem. **54**(26), 10164–10169 (2006).

[26] S. Desplanques, F. Renou, M. Grisel, and C. Malhiac, "Impact of chemical composition of xanthan and acacia gums on the emulsification and stability of oil-in-water emulsions," Food Hydrocoll. **27**(2), 401–410 (2012).

[27] M.P. Traynor, R. Burke, J.M. Frías, E. Gaston, and C. Barry-Ryan, "Formation and stability of an oil in water emulsion containing lecithin, xanthan gum and sunflower oil," Int. Food Res. J. **20**(5), 2173–2181 (2013).

[28] P. Pocan, E. Ilhan, and M.H. Oztop, "Characterization of Emulsion Stabilization Properties of Gum Tragacanth, Xanthan Gum and Sucrose Monopalmitate: A Comparative Study," J. Food Sci. **84**(5), 1087–1093 (2019).

[29] K. Abdolmaleki, L. Alizadeh, S.M. Hosseini, and K. Nayebzadeh, "Concentrated O/W emulsions formulated by binary and ternary mixtures of sodium caseinate, xanthan and guar gums: rheological properties, microstructure, and stability," Food Sci. Biotechnol. **29**(12), 1685–1693 (2020).

[30] L. Zhong, M. Oostrom, M.J. Truex, V.R. Vermeul, and J.E. Szecsody, "Rheological behavior of xanthan gum solution related to shear thinning fluid delivery for subsurface remediation," J. Hazard. Mater. **244**–**245**, 160–170 (2013).

[31] U. Eberhard, H.J. Seybold, M. Floriancic, P. Bertsch, J. Jiménez-Martínez, J.S. Andrade, and M. Holzner, "Determination of the effective viscosity of non-Newtonian fluids flowing through porous media," Front. Phys. **7**(MAY), 1–9 (2019).

[32] M. Cho, S.O. Hong, S.H. Lee, K. Hyun, and J.M. Kim, "Effects of ionic strength on lateral particle migration in shear-thinning xanthan gum solutions," Micromachines **10**(8), (2019).

[33] V. Deepak, and S. Vengadesan, "Droplet Velocity and Film Thickness Studies of an Elongated Taylor Droplet in a Microchannel and Characterization Using Machine Learning," Ind. Eng. Chem. Res. **64**(17), 8908–8921 (2025).

[34] K. Amit, A. Assam, and A. Raj, "Droplet migration through deformable stenosed microchannel: Dynamics and blockage," Phys. Fluids **36**(5), (2024).

[35] S.A. Haider, and A. Raj, "Liquid drops on compliant and non-compliant substrates: an ellipsoid-based fitting for approximating drop shape and volume," Microfluid. Nanofluidics **27**(7), 1–17 (2023).

[36] Rohit, S.A. Haider, and A. Raj, "ANN-aided stiffness characterization of thin membranes using droplet motion," Acta Mech. **235**(2), 565–582 (2024).

[37] A. Raj, R. Halder, P. Sajeesh, and A.K. Sen, "Droplet generation in a microchannel with a controllable deformable wall," Microfluid. Nanofluidics **20**(7), 1–16 (2016).

[38] A. Raj, and A.K. Sen, "Entry and passage behavior of biological cells in a constricted compliant microchannel," RSC Adv. **8**(37), 20884–20893 (2018).

[39] A. Raj, and A.K. Sen, "Flow-induced deformation of compliant microchannels and its effect on pressure–flow characteristics," Microfluid. Nanofluidics **20**(2), 1–13 (2016).

[40] I.C. Christov, V. Cognet, T.C. Shidhore, and H.A. Stone, "Flow rate-pressure drop relation for deformable shallow microfluidic channels," J. Fluid Mech. **841**, 267–286 (2018).

[41] A. Günther, and K.F. Jensen, "Multiphase microfluidics: from flow characteristics to chemical and materials synthesis," Lab Chip **6**(12), 1487–1503 (2006).

[42] L.Y. Chu, A.S. Utada, R.K. Shah, J.W. Kim, and D.A. Weitz, "Controllable monodisperse multiple emulsions," Angew. Chemie - Int. Ed. **46**(47), 8970–8974 (2007).

[43] T.J. Merkel, S.W. Jones, K.P. Herlihy, F.R. Kersey, A.R. Shields, M. Napier, J.C. Luft, H. Wu, W.C. Zamboni, A.Z. Wang, and others, "Using mechanobiological mimicry of red blood cells to extend circulation times of hydrogel microparticles," Proc. Natl. Acad. Sci. **108**(2), 586–

591 (2011).

[44] H. Song, J.D. Tice, and R.F. Ismagilov, “A microfluidic system for controlling reaction networks in time,” Angew. Chemie **115**(7), 792–796 (2003).

Supplementary Files

This is a list of supplementary files associated with this preprint. Click to download.

- Multimedia2EffectofLargerInnerDropletsonTotalTransitTime.mp4
- Multimedia1dropletgenerationrigidcompliant.mp4